

Field-domain spintronics in magnetic semiconductor multiple quantum wellsDavid Sánchez,^{1,2,3} A. H. MacDonald,^{2,3} and Gloria Platero¹¹*Instituto de Ciencia de Materiales de Madrid (CSIC), Cantoblanco, 28049 Madrid, Spain*²*Department of Physics, Indiana University, Bloomington, Indiana 47405*³*Department of Physics, The University of Texas at Austin, Austin, Texas 78712*

(Received 19 July 2001; published 11 December 2001)

We develop a theory of nonlinear growth direction transport in magnetically doped II-VI compound semiconductor multiple-quantum-well systems. We find that the formation of electric field domains can be controlled by manipulating the space dependence of the band electron spin polarization, using its exchange coupling to local moments. We emphasize the importance of band electron spin relaxation in limiting the strength of these effects.

DOI: 10.1103/PhysRevB.65.035301

PACS number(s): 73.21.Cd, 72.25.Dc, 72.25.Mk, 75.50.Pp

I. INTRODUCTION

The giant magnetoresistance effect in magnetic metal multilayers¹ occurs because of the coupling of external magnetic fields to band electron spins through their collective spin polarization. The utility of this effect for information storage and field sensing devices has increased interest in exploring related spin-dependent transport properties in both ferromagnetic and paramagnetic semiconductors. At the same time, progress in the homoepitaxy and heteroepitaxy of magnetically doped semiconductors is creating new possibilities for engineered material geometries in which new spin-dependent transport effects are likely to occur.^{2,3} Large band electron spin polarizations can occur⁴ in diluted magnetic semiconductors (DMS's),⁵ for example, in II-VI compounds with Mn substituted on the group II site. Among the striking phenomena already demonstrated in Mn doped II-VI quantum structures are magnetically tunable quantum well barriers and interwell couplings,⁶ spin-dependent dynamics of polarized excitons in spin superlattices,⁷ optically probed spin coherence,⁸ and the injection of highly polarized spin currents into GaAs/AlGaAs light emitting diodes.⁹ In addition, *n*-doping of wide-gap II-VI magnetic semiconductor quantum wells (Zn_{1-x-y}Cd_xMn_ySe) has been achieved,¹⁰ yielding two-dimensional electron gas (2DEG) systems that are exchange coupled to magnetic ions.¹¹ The exchange interaction J_{sd} between *s* electrons in the conduction band and Mn²⁺ *S* = 5/2 local moments, results in band spin splittings larger than $\hbar\omega_c$, the Landau level splitting. The spin splittings can reach values as high as 20 meV.¹² In fact, complete spin polarization can be achieved in quantum wells at relatively low magnetic fields (~ 1 T).¹³

Although the study of electronic transport properties in DMS heterostructure systems is still in its initial stages, interesting predictions have already been made.^{14,15} The present study is motivated in part by the recent growth of a modulation-doped ZnSe/(Zn,Cd,Mn)Se multiple quantum well (MQW) system.¹⁶ In nonmagnetic MQW systems, growth direction transport phenomenology is enriched by an interplay between charge accumulation and resonant interwell tunneling effects that results in the formation of electric field domains. In this paper we report on a theory of the influence of exchange coupling with Mn ion spins on electric field domain formation and on the sensitivity of this influ-

ence to spin-relaxation rates within the quantum wells.

The formation of electric field domains is the hallmark of dc-biased transport in weakly coupled semiconductor superlattices. Spontaneously generated inhomogeneities in the spatial distribution of voltage drops, were proposed as an explanation for overall conductance [$G(V)$] oscillations,¹⁷ discovered in pioneering growth direction MQW transport studies. This early hypothesis was later confirmed by direct photoluminescence measurements.¹⁸ Subsequently, highly doped GaAs/AlGaAs superlattices that present sawtoothlike current-voltage (*I-V*) characteristics in the negative differential conductance (NDC) region were studied in detail. Along branches of the sawtooth two approximately constant electric field regions develop in the sample, separated by a layer of accumulated electrons. In the following, we follow common usage in referring to these layers with higher 2D electron density as *monopoles*. This nonequilibrium configuration enables resonant tunneling between ground and excited subbands in the high field region, minimizing the total resistance of the superlattice. Increases in external voltage in this regime lead to sharp decreases in current, followed by discrete jumps of the monopole region from a well to its upstream neighbor, extending the high field domain over an additional period and increasing the current.

Past work has studied the dependence of domain formation and evolution on magnetic fields applied along the growth direction and on far-infrared radiation wavelength. In the former case, the formation of Landau levels and scattering between them introduces a new voltage scale for domain formation.¹⁹ In the latter case, photonic sidebands sustain the formation of the electric field domains.²⁰ The inclusion of the electronic spin in the study of perpendicular transport in MQW's can also be expected to alter electric field domain formation physics, and exchange coupling to Mn spins should make it possible to tune these effects with relatively weak external magnetic fields. This is the possibility that we explore at greater length in this paper. In all these cases the electron-electron interaction, although small in the ground state in comparison with typical energies of the system, cannot be neglected since it is the Poisson equation relating charge accumulation to field variations that is at the heart of field-domain formation. For example, it permits the experimentally observed²¹ multistability of distinct stationary

physical states at a fixed bias voltage. Nonetheless, the mean-field Hartree approximation is sufficient to capture this physics in typical samples. The nonlinearity of the current versus voltage relationship between neighboring quantum wells, coupled with the nonlocality of electron-electron interaction effects leads to transport equations that can be solved only numerically, and also to results that are sometimes difficult to interpret.

In this paper we deal with the formation of electric field domains in II-VI MQW systems with one or more (II,Mn)VI quantum wells. The main ingredients of our self-consistent theoretical model are (i) a theory for the tunneling current between two spin-polarized 2DEG's; (ii) a continuity equation that accounts for relaxation of nonequilibrium spin populations; (iii) a relationship between the up and down chemical potentials and their densities; (iv) the application of simple Hartree mean field theory to account for the Coulomb interaction; and (v) a mean-field theory for the interaction between 2DEG electrons and Mn spins whose average polarization is very sensitive to external magnetic fields at low temperature. We shall demonstrate that new features appear in the I - V curve that depend on temperature and Mn spin concentration, and explain why spin bottlenecks turn out to have a strong influence in the instability regions.

The paper is organized as follows. In Sec. II our theoretical model is thoroughly explained. Section III is devoted to a discussion of technical details important for the numerical integration of the rate equations that describe the time dependent charge, spin, and current distributions. In Sec. IV we give numerical results and discuss their interpretation. Finally, Sec. V contains our conclusions.

II. THEORETICAL MODEL

Following successful⁵ early work on bulk systems by Kossut,²² Bastard,²³ and Gaj,²⁴ we account for the presence of Mn ions in DMS quantum wells, by combining a phenomenological exchange model with a virtual crystal approximation and mean-field theory. The lattice parameters and the band Hamiltonian parameters of a II-VI heterostructure are assumed to change smoothly as Mn^{++} spins are introduced in the system and a $S=5/2$ quantum spin is assumed to be added to the low energy degrees of freedom for each Mn spin. The band electron system and the local moments are coupled by a ferromagnetic exchange interaction that favors parallel alignment of the local moment and band electron spins. The total Hamiltonian of the system is

$$\mathcal{H} = \mathcal{H}_0 + \mathcal{H}_T + \mathcal{H}_{\text{scatt}} + \mathcal{H}_{\text{int}}^{ss} + \mathcal{H}_{\text{int}}^{sd} + \mathcal{H}_{\text{int}}^{dd} + \mathcal{H}_{\text{sf}}. \quad (1)$$

The first four terms in the right-hand side of the equation describe a conventional superlattice system with many weakly coupled quantum wells.

(i) \mathcal{H}_0 is the Hamiltonian for independent electrons in N isolated quantum wells. Its energy spectrum is purely single-particle-like, and the quasiparticle spectrum is that of an isolated quantum well 2DEG $\mathcal{E}_j(\vec{k}_{\parallel}) = E_j + \xi(\vec{k}_{\parallel})$, where \vec{k}_{\parallel} is the wave vector parallel to the MQW heterointerfaces, $\xi(\vec{k}_{\parallel}) = \hbar^2 k_{\parallel}^2 / 2m^*$, m^* is the effective mass, and j is the

quantum well subband index. We will take \vec{k}_{\parallel} to be a continuous index, disregarding Landau-level formation in the weak magnetic fields we will consider.

(ii) \mathcal{H}_T contains the tunneling amplitudes that couple quasiparticles in different quantum wells. In weakly coupled superlattices it is a good approximation to treat this term by leading order perturbation theory as we discuss in Sec. II A.

(iii) $\mathcal{H}_{\text{scatt}}$ contains the scattering terms within a quantum well that allow a nonequilibrium quasiparticle to relax its excess energy, but does not contain terms that permit the quasiparticle system to bring its spinsubsystems into equilibrium. (These terms are absorbed in \mathcal{H}_{sf} .) Because it is difficult to describe these scattering processes accurately, or even to know what they are in particular systems, we will use a phenomenological relaxation time approximation. The time scale associated with these processes is typically rather short ($\tau_{\text{scatt}} \sim 0.4$ ps).¹¹

(iv) $\mathcal{H}_{\text{int}}^{ss}$ is the electron-electron interaction in the conduction band for which we will use a Hartree mean-field approximation. (See Sec. II C).

The remaining terms in Eq. (1) describe *spin*-related physics.

(i) $\mathcal{H}_{\text{int}}^{sd}$ is the exchange interaction between s conduction band electrons and Mn local moments, an interaction that turns out to be ferromagnetic in II-VI MQWs. When the mean-field and virtual crystal approximations are employed, the effect of this coupling is to make the subband energies spin-dependent in those quantum wells that contain Mn ions $E_{j \rightarrow} \rightarrow E_j^{\sigma}$.

(ii) $\mathcal{H}_{\text{int}}^{dd}$ represents the antiferromagnetic super exchange interaction between Mn spins on neighboring lattice sites that has been found to be important in modelling bulk DMS systems.⁴ Since our intention here is to address the qualitative physics of field domains in DMS MQW systems, we neglect $\mathcal{H}_{\text{int}}^{dd}$. We do expect, however, that these interactions will be important for detailed modelling of specific experimental systems.

(iii) \mathcal{H}_{sf} contains the microscopic processes that allow equilibrium to be established between spin subsystems within a quantum well. The fact that spin relaxation can be quite slow in the conduction band²⁵ is one of the motivations for this work. Relaxation times in excess of 1 ns have been established experimentally⁸ in II-VI semiconductor QW's without Mn. In II-VI DMS QWs these times are reduced to tens of picoseconds (but still larger than τ_{scatt}).⁴ We discuss the role of these terms at greater length in Sec. II B.

A. 2D-2D tunneling

The standard theory of tunneling relates the electric current between weakly coupled subsystems to tunneling matrix elements and subsystem spectral functions.^{26,27} In our case we will apply this theory to describe the current flowing between one quantum well and its neighbor. Since elastic and inelastic scattering times in the quantum wells are shorter than any other time scale of the problem, we can follow the standard lines of tunneling theory and assume that the electrons in each well are in quasiequilibrium between successive tunneling events and that their temperature is that

of the lattice. We ignore interwell spin-flip processes, so that currents are carried between wells by the two spin subsystems *in parallel*. Accordingly, the current per spin from the i th well to the $(i+1)$ st well is given by the following general expression:

$$J_{i,i+1}^\sigma = \frac{e}{2\pi\hbar} \sum_{\vec{k}, \vec{k}_{i+1}} T_{\vec{k}, \vec{k}_{i+1}}^\sigma \int d\varepsilon A_{\vec{k}_i}^\sigma(\varepsilon) A_{\vec{k}_{i+1}}^\sigma(\varepsilon + eV_i) \times [f(\varepsilon - \mu_i^\sigma) - f(\varepsilon - \mu_{i+1}^\sigma + eV_i)], \quad (2)$$

where $\sigma = (\uparrow, \downarrow)$ is the conduction electron spin index, $T_{\vec{k}, \vec{k}_{i+1}}^\sigma$ is the transmission coefficient between particular wave vector states in the two quantum wells, eV_i is the voltage drop across the i th barrier, and $f(x) = 1/[\exp(x/k_B T) + 1]$ is the Fermi factor. μ_i denotes the chemical potential in well i measured from the bottom of well i . A commonly used Lorentzian-shape function is chosen to represent the influence of disorder on quasiparticles in the j th subband within the i th quantum well:

$$A_{\vec{k}_i}^\sigma(\varepsilon) = \frac{1}{\pi} \frac{\gamma}{[\varepsilon - \mathcal{E}_j^\sigma(\vec{k}_i)]^2 + \gamma^2}. \quad (3)$$

This form for the spectral function results from neglecting the real part of the disorder self-energy, which introduces an unimportant rigid shift of the quasiparticle energies, and the energy dependence of its imaginary part. γ is treated as a phenomenological parameter whose value may vary substantially from sample to sample and is to be taken from experiment. ($\gamma = \hbar/2\tau_{\text{scatt}} \sim 1$ meV). In weakly coupled superlattices the broadening due to scattering is much larger than the miniband width so that tunneling between quantum wells is *sequential* rather than bandlike. In this regime an electron undergoes many scattering events in one well before tunneling to the next well. Because of the epitaxial nature of the samples in question, we assume that the tunneling process conserves parallel momentum, i.e., effects such as interface roughness are not taken into account. This approximation is made for the sake of definiteness and does not influence the qualitative conclusions we will reach. In addition, the typical electronic densities in particular quantum wells are assumed to be $\sim 10^{11}$ cm $^{-2}$ so that only the lowest subband is appreciably populated in the quasiequilibrium state of a quantum well. Therefore, when current flows dominantly by a transition from the ground state of well i to the first excited state in well $i+1$, rapid relaxation to the lowest subband (via, e.g., emission of a LO phonon) is assumed. This simplifications lead us to an analytical expression for Eq. (2) at $T=0$ K:

$$J_{i,i+1}^\sigma = \frac{e\nu_0}{2\pi^2\hbar} \Xi(\mu_i^\sigma, E_{i1}^\sigma, \mu_{i+1}^\sigma, E_{i+11}^\sigma, eV_i) \times \sum_j T_j \frac{2\gamma}{(E_{i1}^\sigma - E_{i+1j}^\sigma + eV_i)^2 + (2\gamma)^2}. \quad (4)$$

The sum in Eq. (4) is extended over all subbands in the $(i+1)$ st well $\nu_0 = m^*/2\pi\hbar^2$ is the 2D density of states per

spin.. The transmission coefficients from the ground subband to the j th subband of the neighboring well T_j are calculated by means of the transfer Hamiltonian method.³⁶ Since this approach involves only orbital degrees of freedom, T_j does not depend explicitly on σ . We are therefore implicitly restricting ourselves to the case when the spin splittings are not so large as to mix different subbands. The function Ξ expresses the width of the energy ‘‘window’’ available for tunneling. For tunneling between the lowest subbands

$$\Xi \equiv \begin{cases} \mu_i^\sigma - E_{i1}^\sigma & : \mu_{i+1}^\sigma - eV_i < E_{i1}^\sigma, \\ -(\mu_{i+1}^\sigma - E_{i+11}^\sigma) & : \mu_i^\sigma + eV_i < E_{i+11}^\sigma, \\ \mu_i^\sigma - \mu_{i+1}^\sigma + eV_i & : \text{otherwise,} \end{cases}$$

where E_{i1} is the first subband energy in the i th well and so on. The expressions for the energy window for tunneling to higher subbands are similar and differ only through the absence of Pauli blocking effects in the target layer.

B. Spin splitting and spin relaxation

The exchange interaction between the conduction band electrons and the Mn $^{2+}$ ions produces a giant spin splitting of the 2DEG even in the presence of a small magnetic field. The bottom of the band for each spin rigidly shifts accordingly:

$$E_j^\sigma = E_j - s\Delta, \quad (5)$$

$$\Delta \equiv J_{sd} N_{\text{Mn}} S B_S \left(\frac{g\mu_B B S}{k_B T_{\text{eff}}} \right), \quad (6)$$

where E_j is the j th miniband center, $s = +(-)$ for $\sigma = \uparrow(\downarrow)$, J_{sd} is the exchange integral, N_{Mn} is the density of Mn $^{2+}$ ions with spin equals to $S = 5/2$, B_S is the Brillouin function, and T_{eff} is an effective temperature which can, in general, include a correction due to antiferromagnetic interactions between neighboring Mn ions.⁴ We have assumed here that the magnetic field (B) orientation is such that the quasiparticle energy is lowered for *up* spins. Note that our virtual crystal approximation for the Mn ions implies that the mean-field experienced by band electrons of spin σ is spatially uniform. In this paper we take the field experienced by the local moments in Eq. (6) to be the external magnetic field. In fact, the mean-field approximation we employ can be extended²⁸ to include the contribution of spin-polarized band electrons to the total effective magnetic field experienced by the local moments. When this is done, ferromagnetism results. That extension of the models and approximations employed here does in fact appear to account for the main features of the carrier induced ferromagnetism that occurs²⁹⁻³¹ in doped diluted ferromagnetic semiconductors. The transition temperatures in these systems can be substantial³² for *p*-type systems and for higher carrier densities. In the case of relatively low-density *n*-type systems, the ferromagnetic transition temperatures will be low and ferromagnetism does not necessarily occur, when direct interactions between the Mn local moments are included in the

theory. Experimentally, most n -type DMS 2DEG's show no evidence for ferromagnetism. In this paper we will assume that the contribution of the spin-polarized conduction band system to the effective field experienced by the Mn local moments is negligible. If ferromagnetism did occur, the non-linear field-domain transport physics we discuss in this paper would be further enriched.

In modelling spin relaxation within a quantum well we start by neglecting the transport currents $J_{i,i+1}^\sigma$.³³ For instantaneous spin splittings smaller than the Fermi energy we use the following phenomenological spin-relaxation rate equation within each quantum well:

$$\frac{dn_i^\sigma}{dt} = -\frac{\mu_i^\sigma - \mu_i^{\bar{\sigma}}}{\tau_{sf}} \nu_0, \quad (7)$$

where $\bar{\sigma}$ is the spin opposite to σ and τ_{sf} is the spin-scattering time. (We neglect the dependence of τ_{sf} on Δ , which may be important in certain samples.¹³) This equation implicitly assumes the linear noninteracting 2DEG relationship between density and chemical potential, so that correlation effects are not taken into account:³⁴

$$n_i^\sigma = \nu_0(\mu_i^\sigma - E_{i1}^\sigma). \quad (8)$$

In the absence of a driving bias voltage, the solution of Eq. (7) at $t \rightarrow \infty$ is $n_i^\uparrow = (n_i + \nu_0 \Delta)/2$ and $n_i^\downarrow = (n_i - \nu_0 \Delta)/2$. Here $n_i = n_i^\uparrow + n_i^\downarrow$ is the total density of carriers in the i th well. We can see from this asymptote that Eq. (7) is valid only for spin splittings smaller than the chemical potential.

For Δ greater than the chemical potential, Eq. (7) must be modified using Eq. (8):

$$\frac{dn_i^\downarrow}{dt} = -\frac{n_i^\downarrow}{\tau_{sf}} = -\frac{\mu_i^\downarrow - E_{i1}^\downarrow}{\tau_{sf}} \nu_0, \quad (9a)$$

$$\frac{dn_i^\uparrow}{dt} = -\frac{dn_i^\downarrow}{dt}. \quad (9b)$$

For large enough Δ , Eq. (9) leads to an equilibrium state with full spin polarization. (See Fig. 1.)

Adding transport currents to these considerations leads to the following discrete continuity equations for the spin population in each quantum well:

$$\frac{dn_i^\sigma}{dt} = \frac{J_{i-1,i}^\sigma - J_{i,i+1}^\sigma}{e} - \frac{\mu_i^\sigma - \mu_i^{\bar{\sigma}}}{\tau_{sf}} \nu_0, \quad i = 1, \dots, N \quad (10)$$

for the case $\mu_i^\uparrow - E_{i1}^\uparrow > 2\Delta$. Otherwise, Eq. (9) must replace the second term on the right-hand side of Eq. (10).

C. Electrostatics

In large area heterostructures, the Coulomb interaction is usually included in a Hartree mean-field approximation. The Poisson equation relates the electrostatic potential drop across MQW barriers, V_i , to the charge distribution among the quantum wells

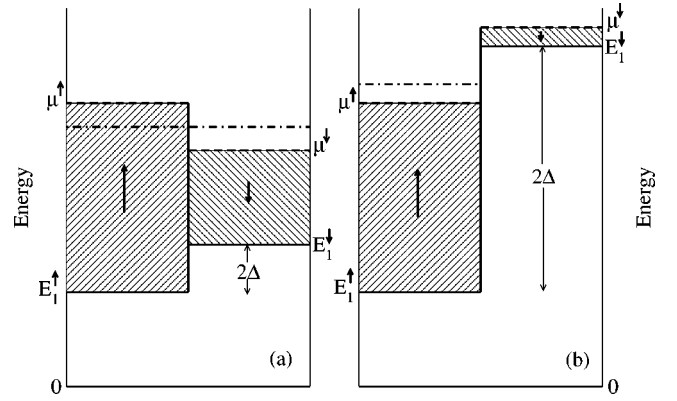


FIG. 1. Schematic illustration of spin relaxation within a quantum well. The dashed lines indicate initial nonequilibrium chemical potentials while the dot-dashed line the equilibrium ($t \rightarrow \infty$) chemical potentials. Panel (a) is for the case of spin splittings smaller than $\mu^\uparrow - E_{i1}^\uparrow$ while panel (b) is the case of for spin splittings larger than $\mu^\uparrow - E_{i1}^\uparrow$ for which the equilibrium state is completely spin polarized. The zero of energy in these plots is the electrostatic potential of the quantum well.

$$\frac{V_i - V_{i-1}}{d} = \frac{e}{\epsilon} (n_i - N_w), \quad i = 1, \dots, N, \quad (11)$$

where d is the superlattice period, ϵ is the sample average permittivity, and N_w denotes the doping density within the wells. (Experimentally, doping is usually accomplished by placing a ZnCl_2 layer in the barrier layers; this difference in electrostatics compared to our model has no important consequences.)¹¹

By inspection of Eqs. (10) and (11) it is obvious that a set of boundary conditions must be provided for n_0 and n_{N+1} . Within our model these layers play the role of source and drain, respectively. A simple way to represent source and drain³⁵ is to fix the density in both layers at high values. We take

$$n_0, n_{N+1} \equiv \kappa N_w, \quad (12)$$

where $\kappa > 1$ is an adjustable parameter. More sophisticated models^{36,37} have proven that a proper description of the contacts can have a strong effect on the selection of the transport equation solution when multistability occurs, especially when dynamical solutions are allowed.³⁷ However, we choose not to delve into these effects in detail here since our main interest is on spin effects. For the sake of definiteness, the contacts are taken to be unpolarized throughout our calculations; including spin-polarized injection in our theory would be straightforward and indeed this may be a very interesting avenue to explore in future experimental and theoretical studies. With this representation of the source and drain, fixing the overall bias voltage

$$V = \sum_{i=0}^N V_i, \quad (13)$$

closes the set of equations.

III. NUMERICAL CONSIDERATIONS

Our model contains $5N+1$ unknown functions of time ($2N$ chemical potentials, μ_i^σ , $2N$ electronic densities, n_i^σ , and $N+1$ voltage drops, V_i). These unknown functions are determined by the $2N$ constitutive equalities [Eq. (8)], $2N$ rate equations [Eq. (10)], N Poisson relations [Eq. (11)], and the total bias condition [Eq. (13)]. Thus, giving a physically sensible initial profile, the system of algebraic-differential equations can be integrated to yield a definite solution. Standard numerical methods are employed in solving Eq. (10), being careful to use the appropriate spin-relaxation equation [either Eq. (7) or Eq. (9)] at each time step.

The total current density $J(t)$ traversing the sample at time t is determined by the following procedure. Differentiate Eq. (11) with respect to time and substitute the result into the sum of Eq. (10) over spin indices in order to eliminate the densities and chemical potentials. This leads to the following current which has the same value when evaluated for any well index i :

$$J(t) = \frac{\epsilon}{d} \frac{dV_i}{dt} + J_{i,i+1}(t). \quad (14)$$

The first term of the right-hand member of the previous equation is the displacement current whereas the second term is the tunneling current $J_{i,i+1}(t) = J_{i,i+1}^\uparrow(t) + J_{i,i+1}^\downarrow(t)$. For static steady state solutions discussed in this paper only the latter term is finite.

IV. RESULTS

We focus on ZnSe/Zn $_{1-x-y}$ Cd $_x$ Mn $_y$ Se DMS MQWs. A value of $x \sim 0.2$ has been chosen to be consistent with barriers (~ 200 meV) sufficiently high to capture more than one subband in the quantum wells. For definiteness, we focus on the case where Mn has been incorporated only in the *central* well of the superlattice. In experimental samples the value of y can be varied over a wide range. We expect that the field-tuned field-domain effects we discuss will be strongest at moderate Mn densities, large enough to give rise to sizable spin splittings but not so large as to increase the spin scattering rate excessively.

The experimental samples reported on in Ref. 16 possess ZnSe barriers too thick (~ 30 nm) for perpendicular transport. Under those conditions, the coefficients T_j are so small that electron tunneling would likely occur via impurity channels in the barriers or through different symmetry points in the host semiconductor band structure, violating the assumptions of our theory. For these model calculations we choose a smaller barrier width $b = 5$ nm. The remaining phenomenological parameters have been fixed on the basis of available experimental data: $w = 10$ nm, $m^* = 0.16m_e$, $N_w = 2 \times 10^{11}$ cm $^{-2}$, $\tau_{sf} = 10$ ps, and $\kappa = 1.5$. w is the well width and κ specifies the source and drain densities [see Eq. (12)].

In Sec. IV A we study self-consistent steady-state solutions for low voltages. This will help us understand the more complicated behaviors that result from instabilities in the NDC voltage regime. (See Sec. IV B below.)

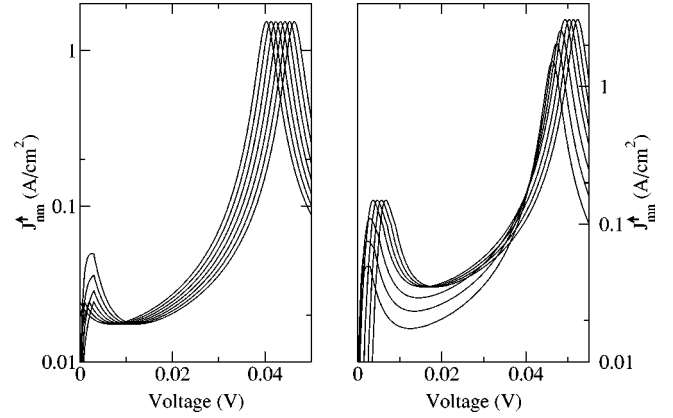


FIG. 2. (a) Current density flowing from a nonmagnetic well to a magnetic one for $\Delta = 0-6$ meV in steps of 1 meV. The rightmost curve corresponds to $\Delta = 0$ meV. (b) Same as (a) but the carriers are now flowing from the magnetic well to the nonmagnetic one. The leftmost curve is for $\Delta = 0$ meV.

A. Linear regime

The behavior of the spin-dependent current density in Eq. (4) depends on many variables. In Figs. 2 and 3 we have plotted $J_{i,i+1}^\sigma$, for the case where μ_m^\uparrow and μ_m^\downarrow have been set to their equilibrium values ($\mu_m^\uparrow = \mu_m^\downarrow = \mu_m$). Thus the spin-dependent chemical potential, measured from the bottom of the well, will depend on the value of Δ (see Fig. 1).

Figure 2(a) plots the up-spin current from a nonmagnetic well to a magnetic one J_{nm}^\uparrow , i.e., net electron flow from a magnetic well to a nonmagnetic one. For $\Delta = 0$ meV and low voltages the behavior is ohmic, as expected. A larger bias results in the alignment of the ground states of both wells within γ , giving rise to a first maximum in the current. After this bias is exceeded, Eq. (4) implies the appearance of a NDC region due to subband mismatch and of a second peak at higher biases when the first subband is aligned with the second subband of the next well. Increasing Δ decreases the value of the first peak since the up-spin density in the magnetic well increases and fewer states are available for tunneling. The peak corresponding to tunneling from first

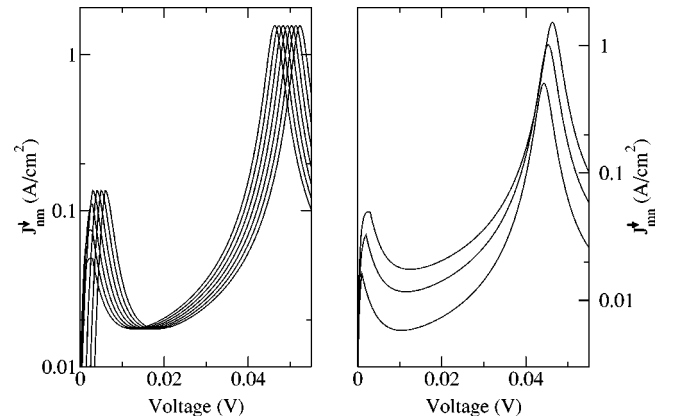


FIG. 3. (a) Same as Fig. 2(a) for down spins. The leftmost curve corresponds to $\Delta = 0$ meV. (b) Same as Fig. 2(b) for down spins. The rightmost curve is for $\Delta = 0$ meV.

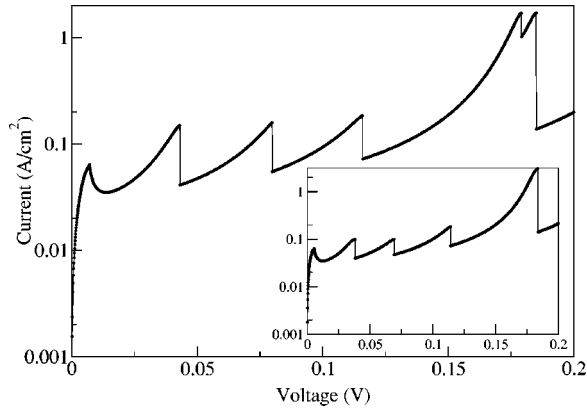


FIG. 4. I - V characteristics for $\Delta = 3$ meV. The first peak occurs near where the first \rightarrow first subband resonant condition occurs in a configuration with no field domains. The following three branches reflect steady states with monopoles in one of the three quantum wells of the system. The monopoles move upstream with increasing bias voltage, increasing the number of high field barriers. Note that the final peak in the I - V curve is split in the spin-dependent transport case. Results for the $\Delta = 0$ meV case are shown in the inset for comparison. The vertical lines that connect different branches of the I - V curve are guides to the eye.

\rightarrow second subband is not affected in magnitude but its position is shifted to lower bias voltages because the bottom of the up-spin subband goes down. For a given value of the spin splitting ($\Delta \sim 3$ meV), the magnetic well is fully polarized so that the first peak magnitude can no longer vary its value, a displacement due to subband lowering is observed instead. In Fig. 2(b) the up-spin current from a magnetic well to a nonmagnetic one is shown. Here the first peak becomes larger as μ_m^\uparrow grows since more electrons take part in the tunneling. This increase ceases once the fully polarized situation is achieved. In addition larger voltages are needed to align the energy levels as Δ increases and the peak moves to higher voltages. Field-domain physics is at heart controlled by the interplay of electrostatics and the layer-to-layer nonlinear I - V relationships. These examples illustrate that the layer-to-layer nonlinear I - V 's can be altered by Δ (and hence an external magnetic field) when one of the layers contains Mn local moments. It follows that the field-domain structure must be Δ and field dependent as we show below.

The corresponding down-spin current is plotted in Fig. 3. The considerations explained above for the up spin case may be invoked to understand this figure. For $\Delta \gtrsim 3$ meV [see Fig. 3(b)] the down-spin current flowing from the magnetic to the nonmagnetic well (J_{mn}^\downarrow) vanishes for any value of the applied bias since in the fully polarized regime, no down-spin carriers are present in the magnetic well.

A numerical calculation for $N = 3$ gives rise to the MQW current-voltage characteristics shown in Fig. 4. Δ has been set to 3 meV. At low voltages the behavior is linear, up to the peak which marks alignment to within $\sim \gamma$ of the first subbands of all wells. Then, after entering the NDC region, an increase of the current occurs because an electric field domain has formed. The underlying mechanism can be understood in the following terms. As the voltage is increased, the

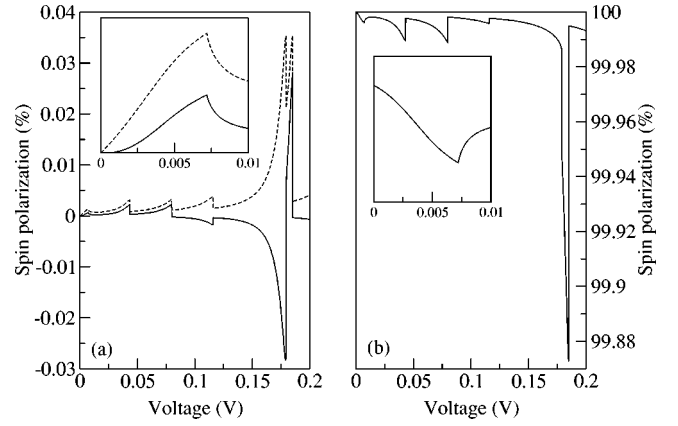


FIG. 5. (a) Spin polarization for the upstream (downstream) quantum well is represented by full (dashed) lines. The inset highlights the low voltage regime. (b) Same as (a) but for the magnetic quantum well.

system prefers to maintain regions of low and high electric fields where intrasubband and intersubband resonant tunneling can occur, rather than maintaining a constant field. The high field regime forms in the downstream side of the sample. In this way, the superlattice minimizes the total resistance and current increases. In order to build the inhomogeneous field, according to Poisson equation (11) an excess electron density, or a monopole, must accumulate in the well at the boundary between low and high field regions. As the voltage is further increased, configurations with particular monopole locations successively become unstable and the monopole moves by one quantum well to increase the width of the high field region. Monopole motion gives rise to an abrupt decrease of the current, which is followed by a gradual increase as the voltage increases further. These successive monopole position jumps lead ultimately to the sawtoothlike I - V curve shape of Fig. 4. The inset in this figure shows the corresponding $\Delta = 0$ meV I - V curve for comparison. The most obvious change is the appearance of a new branch that develops close to the first \rightarrow second subband transition (see below).

The somewhat complicated behavior of the bias voltage dependence of the steady state spin polarization is depicted in Fig. 5 for $N = 3$ and $\Delta = 3$ meV. Notice that in Fig. 5(a) a nonzero steady state spin polarization is induced in the nonmagnetic wells by the spin-dependent transport currents. We have assumed here that the spin-relaxation time constant τ_{sf} is the same in all quantum wells (10 ps). In practice these times are likely to be considerably larger in the nonmagnetic wells, and the induced spin-polarization in these wells will have an even larger importance. For low voltages, the inset of Fig. 5(b) shows a reduction of the magnetic well spin polarization. This effect can be understood by realizing that the minority spin current from a nonmagnetic well to a magnetic one J_{nm}^\downarrow grows when the system is driven out of equilibrium by a small bias voltage. This occurs also in J_{nm}^\uparrow but at a smaller rate because of the spin subband displacement in the magnetic well [compare Figs. 2(a) and 3(a)]. Therefore, at low voltages the magnetic well polarization must decrease. Correspondingly, the upstream-well polarization must in-

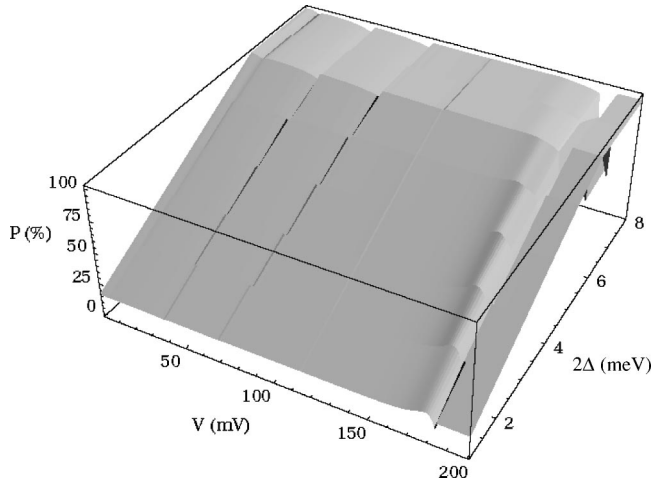


FIG. 6. 3D plot describing the dependence of the magnetic well spin polarization on voltage bias and spin splitting Δ . In constructing this figure, τ_{sf} has been increased to 10 ns (still a reasonable value) (Ref. 8) in order to magnify the effects commented on the text.

crease [see the inset of Fig. 5(a)] since down spins leak out of it. The enlargement of the downstream-well spin polarization has the same origin. [See Figs. 2(b) and 3(b).]

B. NDC regime

As explained above, once the bias voltage reaches the NDC regime, electric field domains form in the sample. As we now discuss, their formation strongly influences spin-polarizations in both magnetic and nonmagnetic quantum wells, with discontinuities associated with every break in the I - V curve. The magnetic well polarization, P , varies particularly strongly, especially when the monopole moves through the magnetic well, and becomes stronger as the spin splitting is increased. This can be seen in Fig. 6, which describes the general behavior of P with voltage and spin splitting.

If Δ is further increased ($\Delta = 6$ meV), new branches appear in the I - V curve (see Fig. 7). The extra branch that

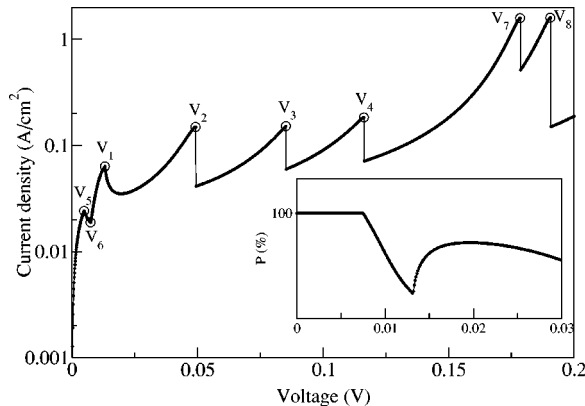


FIG. 7. I - V characteristics for $\Delta = 6$ meV. Note the appearance of new branches in the steady-state I - V curve. The spin polarization in the magnetic quantum well at low voltages is plotted in the inset.

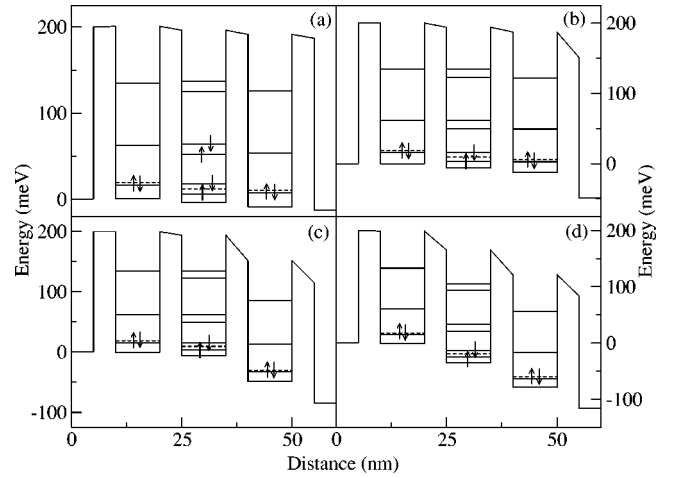


FIG. 8. MQW profiles for V_1 , V_2 , V_3 , and V_4 [(a), (b), (c), and (d), respectively] marked in Fig. 7. Resonant levels (chemical potentials) are depicted by solid (dashed) lines. The spin polarizations plotted in Fig. 5(a) are not observable on the scale of these figures.

appeared close to the $E_1 \rightarrow E_2$ transition at smaller Δ is now fully developed. In addition, a new branch forms *before* the $E_1 \rightarrow E_1$ transition.

To better understand the subtle interplays that control these features, we have studied the self-consistent steady-state well-dependent spin polarizations at the particular voltages marked in Fig. 7. The series of MQW electrostatic profiles illustrated in Fig. 8 are dominated by classical field-domain physics not qualitatively influenced by the spin-dependent nature of the transport. Figure 8(a) (V_1) is the highest voltage at which intrasubband ($E_1 \rightarrow E_1$) resonant tunneling can be maintained. The electric field drops almost linearly along the system. In Fig. 8(b) (V_2) the formation of a high electric field domain in the last barrier is clearly observed, favoring a resonant condition between the third well and the collector first-excited subband.³⁸ The second branch in the NDC region (V_3) involves the generation of a larger high field domain [see Fig. 8(c)]. The domain wall is now located in the magnetic well. A jump to the first well [Fig. 8(d)] (V_4) is accompanied by further expansion of the high field domain. In this situation all tunneling within the wells takes place between the ground and the excited states, followed by a rapid relaxation to the first subband.

Figure 9 illustrates spin populations near I - V features where the spin-dependent element introduced by the magnetic quantum well plays a qualitative role. Figure 9(a) describes the position of energy levels for the voltage V_5 marked in Fig. 7. The subband energies in the nonmagnetic wells (E^\uparrow and E^\downarrow) are quasidegenerate. Notice that resonant tunneling occurs between E_{11}^\uparrow and E_{21}^\downarrow . Further increase of the voltage, however, results in a decrease of the current since now $E_{11}^{\uparrow,\downarrow}$ is then off-resonance [see Fig. 9(b)]. The current is then increased again since E_{11}^\downarrow starts to match E_{21}^\downarrow . This explains why P does not show the behavior observed for smaller Δ ($\Delta = 3$ meV) in the linear regime. [In contrast to the inset of Fig. 5(b), the inset of Fig. 7 presents a flat polarization at low voltages.] P starts to increase only when V is such that E_{11}^\uparrow reaches within γ of E_{21}^\downarrow . The splitting of

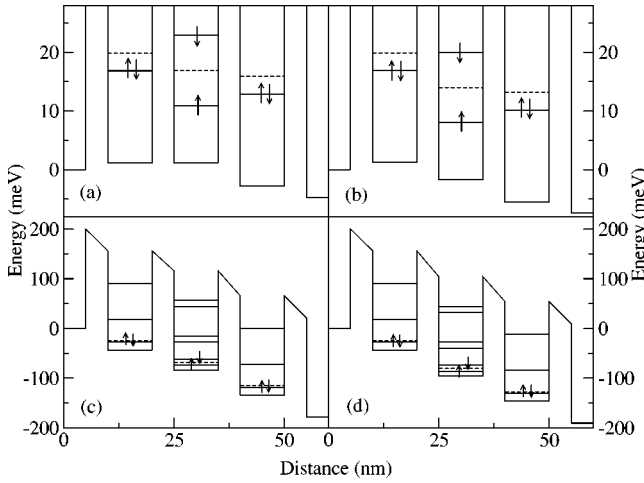


FIG. 9. Same as Fig. 8 for V_5 , V_6 , V_7 , and V_8 [(a), (b), (c), and (d), respectively].

the branch at higher bias voltage where all transport occurs via intersubband ($E_1 \rightarrow E_2$) resonant tunneling has a similar explanation. Figure 9(c) is stabilized by alignment of E_{11}^\uparrow with E_{22}^\downarrow levels. Subband mismatch at higher bias gives rise to a sharp reduction of the current, which increases later, as the voltage is increased and resonant tunneling between E_{11}^\downarrow and E_{22}^\downarrow levels is achieved. Incidentally, the dips in P illustrated in Fig. 5 can be explained in this way. When the latter alignment occurs, a large flow of down-spin carriers streams towards the magnetic well, causing a sharp decrease of the polarization. The remaining features in Fig. 5 can be understood in similar terms.

So far all results were calculated by sweeping voltages up. Steady state solutions in the NDC bias voltage region are in general multistable. We can obtain different solutions at a given bias voltage by evolving solutions following different histories,²¹ for example, by decreasing voltages from a high initial bias. For a given voltage different values of the current with different density and spin polarization profiles may be achieved. To amplify effects, in studying this possibility, we have set $\tau_{sf} = 10$ ns in a $N=9$ superlattice. The change in P with voltage is now so greatly increased (see Fig. 10) that even *reversed* polarization can be observed at somewhat larger values of τ_{sf} in the $E_1 \rightarrow E_2$ resonant tunneling regime (not shown here). This is a direct consequence of the emergence of dominant spin bottlenecks.³⁹ The alterations in polarization are more visible for voltages greater than the one corresponding to the $E_1 \rightarrow E_2$ resonance, but we choose not to show them here since these involve transitions to higher excited energy levels, close to the top of the barrier, where our model breaks down. However, for sufficiently high barriers it would be natural to obtain such behavior.

Figure 10 shows three different values of spin polarization in the magnetic well which can be obtained at a particular bias voltage, depending on the sample history, up sweep from zero voltage, down sweep from a high voltage, and up sweep to an intermediate voltage followed by down sweep. We emphasize that this kind of hysteretic phenomena between magnetic states is driven here by *electric* fields.

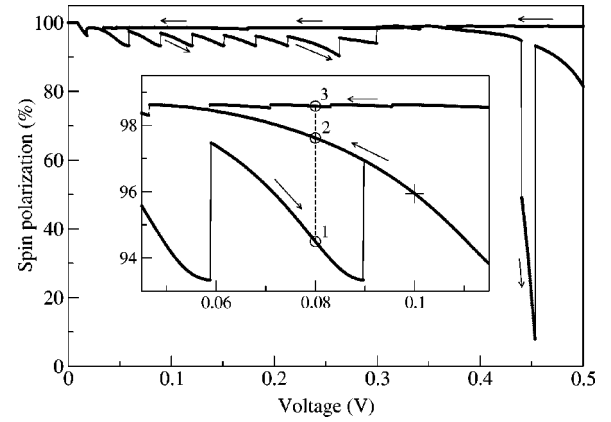


FIG. 10. Multistability of distinct polarization steady states within the magnetic well of a $N=9$ MQW system. The inset shows a blow-up of three different steady states reached at $V=0.08$ meV. The state labeled 1 (3) is achieved by sweeping voltage up (down) from a high (low) initial bias. The state labeled 2 is obtained by sweeping voltage up to $V=0.1$ (marked with a cross) and then reversing the sweep direction.

V. CONCLUSION

We have introduced and studied a simple model for growth direction nonlinear transport in multiple quantum well systems containing magnetically doped layers. Our analysis is based on a tunneling Hamiltonian expression for the current between spin-polarized quantum wells and on a phenomenological expression for spin relaxation within quantum wells. Numerical studies of this model show that it predicts rich behavior due to its nonlinearity and due to the additional degrees of freedom introduced by spin-dependent transport. Nonlinearity manifests itself in the formation of electric field domains when the differential conductivity between neighboring layers is negative. We find that the spin polarization of electrons in magnetic wells can change substantially when the system jumps between different branches of the I - V curve. When current flows finite electron spin polarization extends from the magnetic quantum wells to nonmagnetic quantum wells. When large equilibrium spin splitting, the I - V curve is strongly affected by the appearance of extra branches, due to tunneling into and out of spin polarized well subbands and these effects become more and more prominent when the characteristic time for spin-relaxation is longer.

The effects addressed in this paper could be investigated experimentally by studying transport properties and by studying the polarization dependence of interband optical absorption and photoluminescence in MQW systems containing magnetically doped layers. The predicted sensitivity of transport properties to external magnetic fields, suggests that these systems could potentially be useful for magnetic field sensors, most likely in geometries with a relatively small number of quantum wells. The sensitivity to external fields will be strongest at low temperatures where the Mn ions are easily polarized to produce the maximum equilibrium spin-splitting field. To illustrate the sort of effects that we expect to occur, we have considered only relatively simple geometries with a single magnetic layer. Other effects will

occur in larger MQW systems with particular geometries. In general there is considerable latitude for designing the Mn density distribution in the MQW system to realize desired magnetoresistance effects that could be described with the type of model we have introduced here.

Analogous of the magnetotransport effects we discuss will also occur in ferromagnetic multiple quantum well systems, similar to the delta-doped layered (Ga,Mn)As systems studied by Kawakami *et al.*⁴⁰ These systems are ferromagnetic and the carriers are holes rather than electrons, leading to strain-sensitive spin-orbit-coupling induced magnetic anisotropy^{29,41} and coercivities. These properties suggest a rich interplay between the hysteretic magnetoresistance effects common in thin film itinerant electron magnets^{1,42} and the hysteretic effects discussed here, which have their roots in electric field domain structures.⁴³ Had ferromagnetism been taken into account in our model calculations, by solving

for Δ self-consistently in Eq. (6), not only the electric field domain structure but also the magnetic state configuration would have been sensitive to the bias voltage history. Exploring these possibilities appears to be a promising avenue for future experimental and theoretical work.

ACKNOWLEDGMENTS

One of us (D.S.) thanks the hospitality of Indiana University and The University of Texas at Austin where most of this work was completed. This work was supported by the Spanish DGES Grant No. PB96-00875, by the European Union TMR Contract FMRX-CT98-0180, and by the Indiana 21st century fund, the Welch Foundation and DARPA/ONR Award No. N00014-00-1-0951. The authors acknowledge valuable assistance from Tomas Jungwirth.

-
- ¹M.N. Baibich, J.M. Broto, A. Fert, F. Nguyen Van Dau, F. Petroff, P. Eitenne, G. Creuzet, A. Friederich, and J.C. Chazelas, *Phys. Rev. Lett.* **61**, 2472 (1988); G. Binash, P. Grünberg, F. Saurenbach, and W. Zinn, *Phys. Rev. B* **39**, 4828 (1989).
- ²J.-Ph. Ansermet, *J. Phys. C* **10**, 6027 (1998).
- ³H. Ohno, *Science* **281**, 951 (1998).
- ⁴D.D. Awschalom and N. Samarth, *J. Magn. Magn. Mater.* **200**, 130 (1999).
- ⁵P. Kacman, *Semicond. Sci. Technol.* **16**, R25 (2001); J.K. Furdyna and J. Kossut, *Diluted Magnetic Semiconductors*, Vol. 25 of *Semiconductor and Semimetals* (Academic Press, New York, 1988); T. Dietl, *Diluted Magnetic Semiconductors*, Vol. 3B of *Handbook of Semiconductors* (North-Holland, New York, 1994).
- ⁶J. Kossut and J.K. Furdyna, in *Diluted Magnetic (Semimagnetic) Semiconductors*, edited by R.L. Aggarwal, J.K. Furdyna, and S. von Molnar (Materials Research Society, Pittsburgh, 1987).
- ⁷J.F. Smyth, D.A. Tulchinsky, D.D. Awschalom, N. Samarth, H. Luo, and J.K. Furdyna, *Phys. Rev. Lett.* **71**, 601 (1993).
- ⁸J.M. Kikkawa, I.P. Smorchkova, N. Samarth, and D. D. Awschalom, *Science* **281**, 1284 (1997).
- ⁹R. Fiederling, M. Keim, G. Reuscher, W. Ossau, G. Schmidt, A. Waag, and L. W. Molenkamp, *Nature (London)* **402**, 787 (1999).
- ¹⁰I.P. Smorchkova, N. Samarth, J.M. Kikkawa, and D.D. Awschalom, *Phys. Rev. Lett.* **78**, 3571 (1997).
- ¹¹I.P. Smorchkova and N. Samarth, *Appl. Phys. Lett.* **69**, 1640 (1996).
- ¹²S.A. Crooker, E. Johnston-Halperin, D.D. Awschalom, R. Knobel, and N. Samarth, *Phys. Rev. B* **61**, R16 307 (2000).
- ¹³S.A. Crooker, D.A. Tulchinsky, J. Levy, D.D. Awschalom, R. Garcia, and N. Samarth, *Phys. Rev. Lett.* **75**, 505 (1995).
- ¹⁴J.C. Egues, *Phys. Rev. Lett.* **80**, 4578 (1998).
- ¹⁵Y. Guo, B. Gu, H. Wang, and Y. Kawazoe, *Phys. Rev. B* **63**, 214415 (2001).
- ¹⁶J.J. Berry, R. Knobel, O. Ray, W. Peoples, and N. Samarth, *J. Vac. Sci. Technol. B* **18**, 1692 (2000).
- ¹⁷L. Esaki and R. Tsu, *IBM J. Res. Dev.* **14**, 61 (1970).
- ¹⁸H.T. Grahn, R.J. Haug, W. Müller, and K. Ploog, *Phys. Rev. Lett.* **67**, 1618 (1991).
- ¹⁹T. Schmidt, A.G.M. Jansen, R.J. Haug, K. von Klitzing, and K. Eberl, *Phys. Rev. Lett.* **81**, 3928 (1998).
- ²⁰R. Aguado and G. Platero, *Phys. Rev. Lett.* **81**, 4971 (1998).
- ²¹J. Kastrup, H.T. Grahn, K. Ploog, F. Prengel, A. Wacker, and E. Schöll, *Appl. Phys. Lett.* **65**, 1808 (1994).
- ²²J. Kossut, *Phys. Status Solidi B* **78**, 537 (1976).
- ²³G. Bastard, *J. Phys. (France)* **39**, 87 (1978).
- ²⁴J. Gaj, *Phys. Status Solidi B* **89**, 655 (1978).
- ²⁵M.E. Flatté and J.M. Byers, *Phys. Rev. Lett.* **84**, 4220 (2000).
- ²⁶G.D. Mahan, *Many-Particle Physics*, 3rd ed. (Kluwer Academic/Plenum Publishers, New York, 2000), Sec. 8.6.
- ²⁷L. Zheng and A.H. MacDonald, *Phys. Rev. B* **47**, 10 619 (1993).
- ²⁸B. Lee, T. Jungwirth, and A.H. MacDonald, *Phys. Rev. B* **61**, 15 606 (2000).
- ²⁹T. Dietl, H. Ohno, F. Matsukura, J. Cibert, and D. Ferrand, *Science* **287**, 1019 (2000).
- ³⁰J. König, H.H. Lin, and A.H. MacDonald, *Phys. Rev. Lett.* **84**, 5628 (2000).
- ³¹J. König, H.H. Lin, and A.H. MacDonald, in *Interacting Electrons in Nanostructures*, edited by R. Haug and H. Schoeller, Lecture Notes in Physics, Volume 579 (Springer, Berlin, 2001).
- ³²H. Ohno, *J. Magn. Magn. Mater.* **200**, 110 (1999).
- ³³A.H. MacDonald, *Phys. Rev. Lett.* **83**, 3262 (1999).
- ³⁴A.H. MacDonald, in *Statistical and Dynamical Aspects of Mesoscopic Systems (Proceedings of the XVI Sitges Conference)*, edited by D. Reguero, G. Platero, L.L. Bonilla, and J.M. Rubí (Springer-Verlag, Berlin, 2000).
- ³⁵L. L. Bonilla, in *Nonlinear Dynamics and Pattern Formation in Semiconductors and Devices*, edited by F.-J. Niedernostheide (Springer, Berlin, 1995), p. 1.
- ³⁶R. Aguado, G. Platero, M. Moscoso, and L.L. Bonilla, *Phys. Rev. B* **55**, R16 053 (1997).
- ³⁷L.L. Bonilla, G. Platero, and D. Sánchez, *Phys. Rev. B* **62**, 2786 (2000).
- ³⁸Actually this is not a realistic case since in an experimental sample the contacts are 3D regions. Thus the boundary condition

- of Eq. (12) fails to account for the experimental evidence: the number of branches in the I - V characteristic is *not* equal to the number of wells. Proper description of the contact regions (Refs. 36,37) results in a good agreement with the experiment. However, Eq. (12) is qualitatively a good starting point.
- ³⁹T. Jungwirth and A.H. MacDonald, *Solid State Commun.* **108**, 127 (1998).
- ⁴⁰R.K. Kawakami, E. Johnston-Halperin, L.F. Chen, M. Hanson, N. Guébels, J.S. Speck, A.C. Gossard, and D.D. Awschalom, *Appl. Phys. Lett.* **77**, 2379 (2000); J. Fernandez-Rossier and L.J. Sham, cond-mat/0106548 (unpublished).
- ⁴¹R. Abolfath, J. Brum, T. Jungwirth, and A.H. MacDonald, *Phys. Rev. B* **63**, 054418 (2001); T. Dietl, H. Ohno, and F. Matsukura, *ibid.* **63**, 195205 (2001).
- ⁴²For recent studies of magnetoresistance effects in ferromagnetic semiconductor thin film systems see M. Tanaka and Y. Higo, *Phys. Rev. Lett.* **87**, 026602 (2001).
- ⁴³This effect differs qualitatively from the electric-field control of the microscopic properties of ferromagnetic semiconductors recently demonstrated by H. Ohno, D. Chiba, F. Matsukura, T. Omiya, E. Abe, T. Dietl, Y. Ohno, and K. Ohtani, *Nature (London)* **408**, 944 (2000).